ISSN: 0067-2904

The landform Deformation at the Iraq-Iran Border due to Earthquakes in the Period (2017-2018)

Baqer H. Sayyid[1*], Auday H. Shaban[1], Najah A. Abd[2]
[1] *Department of Remote Sensing and GIS, College of Science, University of Baghdad, Baghdad, Iraq*
[2]*Department of Geology, College of Science, University of Baghdad, Baghdad, Iraq*

Received: 14/5/2023 Accepted: 1/8/2023 Published: 30/9/2024

Abstract

The study targets to assess the potential of Interferometric Synthetic Aperture Radar (InSAR) in detecting ground distortion caused by earthquakes. The inSAR technique integrates Synthetic Aperture Radar (SAR) and interferometry to reveal the slightest changes on the earth's surface through a specified period, impregnable to climate or time of day. The research analyses some scholarly articles to demonstrate the interest of InSAR in examining earthquakes and their outcome. These articles demonstrate the practical application of InSAR in enhancing fault slip analysis, ground deformation assessment, and early post-seismic changes in earthquakes. InSAR is beneficial with measurements from other tools, such as GPS and time series analysis, but it still offers valuable insights into earthquake characteristics and associated effects. The insights from these methodologies can help devise solutions to mitigate the impacts of earthquakes. In addition, the paper presents information about three earthquake swarm events and their corresponding fault types. The first event occurred on November 12th, 2017, while the second happened on November 25th, 2018. Despite their differences in magnitude and location, the second event was associated with a strike-slip fault. InSAR provides extensive practical applications, from natural hazard monitoring to infrastructure projects and topographic mapping.

Keywords: InSAR, DInSAR, Interferogram, Deformation, Swarm, Displacement.

تشوه التضاريس على الحدود العراقية الإيرانية بسبب الزلازل في الفترة (2017-2018)

باقر حسين سيد[1]*, عدي حاتم شعبان[1], نجاح عبد الحسن عبد[2]
[1]قسم التحسس النائي ونظم المعلومات الجغرافية, الكلية العلوم, الجامعة بغداد, بغداد, العراق
[2]قسم علم الارض, الكلية العلوم, الجامعة بغداد, بغداد, العراق

الخلاصة

يتناول هذا البحث استخدام تقنية رادار الفتحة التركيبية (InSAR) لاكتشاف التشوهات التي تحدث على سطح الأرض نتيجة للزلازل. إن InSAR هي تقنية جيوديسية تجمع بين رادار الفتحة الاصطناعية (SAR) وتقنية التداخل، والتي تمكّن من اكتشاف التغيرات الصغيرة في التشوهات السطحية عبر الزمن بغض النظر عن ظروف الطقس أو وقت اليوم. يتناول البحث خمسة مقالات استخدمت InSAR لتحليل الزلازل وتأثيراتها. تبيّن هذه المقالات فعالية InSAR في تحليل الزلازل، وتوفير فهم عميق لانزلاق الأخطاء وتشوهات الأرض والتغيرات الزلزالية المبكرة. باستخدام InSAR بالتزامن مع تقنيات القياس الأخرى مثل نظام تحديد المواقع

* Email : baqer.ali@sc.uobaghdad.edu.iq

العالمي (GPS) وتحليل السلاسل الزمنية، يمكن للباحثين الحصول على فهم أشمل لخصائص الزلازل وتأثيراتها. تساهم نتائج هذه الدراسات في وضع تدابير فعالة للتخفيف من آثار الزلازل. بالإضافة إلى ذلك، يتناول البحث تفاصيل حول حدثين زلزاليين وأنواع الأخطاء المرتبطة بهما. حدث الأول في 12 نوفمبر 2017، والثاني في 25 نوفمبر 2018. وعلى الرغم من اختلاف قوتهما ومواقعهما، فقد ارتبط الحدث الثاني بانزلاق الأخطاء. في النهاية، تُظهِر النتائج أن InSAR لديه تطبيقات واسعة المدى، من مراقبة المخاطر الطبيعية إلى رسم الخرائط الطبوغرافية وتنفيذ مشاريع البنية التحتية.

1. Introduction

The process known as InSAR is a widely-used remote sensing procedure that offers critical analytical insights into seismic activity. Ground deformation brought about by such activity is monitored via InSAR, with essential information detailing the location, magnitude, and timing of earthquakes being discovered [1]. With the support of pairs of distinct radar images surrounding the same area [2], notably the ability to measure shifts in terrain on a large scale, InSAR provides a broader picture of the extent of deformation in the surface when an earthquake strikes, especially in the context of faults that can be spread out over vast distances [3]. Furthermore, spatial transformations analyzed through InSAR measurements are essential for gauging earthquake activity's exact location and degree [4]. Numerous locations, including Japan, California, and the Himalayas, have employed InSAR to analyze seismic activity. In the earthquake aftermath, it is possible to assess the damage caused and speculate on where the tragedy occurred via InSAR measurements [5]. This procedure assists with identifying the magnitude of the earthquake and its location [6]. InSAR is a valuable approach to monitoring post-earthquake deformation, aiding in hazard and risk appraisals, and helping guide post-disaster recovery operations [7]. In essence, the implications of InSAR deformation measurement are potentially far-reaching regarding earthquake research and hazard management [8].

1.2. Related work

This research examines several studies that explore the use of InSAR technology in detecting ground distortions caused by earthquakes. The review includes five articles that discuss the application of InSAR technology to analyze earthquakes and their effects. [9] One of the studies estimates the co-seismic fault slip of the 2008 Mw 7.9 Wenchuan earthquake through InSAR and GPS measurements. [10]suggested a new technique for InSAR analysis that considers ground motion, atmospheric noise, and orbital errors. [11] other studies employ InSAR to analyze earthquakes' before-earthquake and early after-earthquake deformation in China. [12] Lastly, this review includes a study that used 2D InSAR observation to investigate the before-earthquake and after-earthquake ground deformation caused by an earthquake in Greece and its influence on the deformations of Wall Relic City of the Heraklion.

The researchers illustrated how InSAR technology can be applied to support earthquake analysis by show information on fault slip, ground deformation, and early post-seismic deformation. Integrating InSAR with other measurement techniques like GPS and time series analyses can give researchers a thorough understanding of earthquake characteristics and consequences [13]. This analysis leads to valuable insights that help expand effective methods to reduce earthquake harm.

1.3. Study area

The provinces of Diyala and Sulaymaniyah are located in the Northern of Iraq and are enclosed by mountains and valleys. The province of Diyala covers a zone of 17,685 km^2 and is intersected via the Diyala River, an important tributary of the Tigris. In contrast, the

province of Sulaymaniyah spans 15,074 km^2 and is drained via the Little Zab River [14]. Both areas feature a variety of landscapes, including mountains, hills, valleys, basins, plains, and deserts. The geology of the area is categorized into three regions: the northern and northwestern regions, the northeastern region, and the southern region [15]. Sedimentary rocks, volcanic rocks, and alluvial deposits primarily constitute the northern and northwestern regions. The northeastern region mainly comprises sedimentary rocks, volcanic rocks, and metamorphic rocks [16]. The southern local essentially comprises transformative rocks alongside a few sedimentary and volcanic rocks. Both provinces have mountains, slopes, valleys, fields, and desert regions, Figure (1).

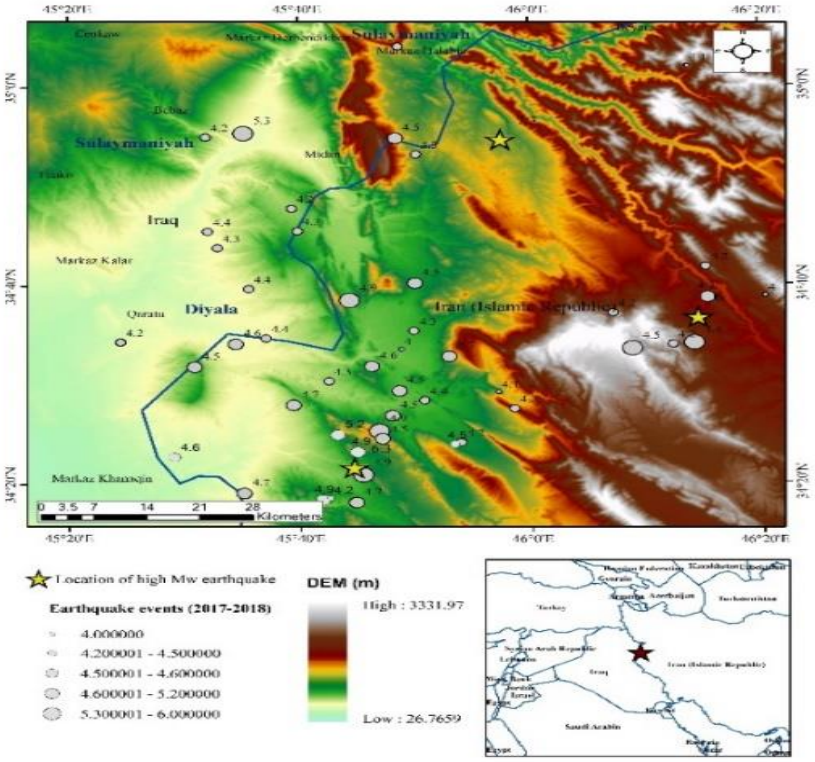

Figure 1: Study area

1.3.1. Seismicity of the study area

The Sulaymaniyah and Diyala locales in Iraq and known for their successive tremors. The essential justification behind the seismic movement in Sulaymaniyah is the Zagros fault Zone located along the Iraq-Iran border. The Diyala fault Zone in northeastern Iraq brings about seismic action in Diyala. Both tectonic and local sources contribute to the seismic activity in the region, including the Zagros Fault Zone, Diyala Fault Zone, and Dehloran Fault Zone [17]. Local sources such as petroleum fields, dams, and infrastructure play a role. Studies indicated that Diyala experiences more frequent and intense earthquakes than Sulaymaniyah due to its location in an area of high tectonic strain [17].

2. Dataset

2.1. Satellite images dataset

Sentinel-1 is a Pleiad of two imaging radar satellites operated by the ESA. The Sentinel-1 mission involves two polar-orbiting satellites equipped with a C band SAR instrument, which acquires data regardless of weather or daytime. The SAR instrument provides all-weather imaging capabilities [18]. The imagery data is rapidly monitored and added to the Google Earth Engine archive, relieving users of the responsibility of searching, downloading, pre-

processing, and georeferencing[19]. Sentinel data is accessible, complete, and open for public use under EU regulations. It offers many data products, including single- and multi-look images, mosaics, change detection, and vegetation indices [20]. The spatial resolution of the images ranges from 2.7×22 to 3.6×22 and 20×22 m [21]. The data can be used for various applications such as ship detection, land cover mapping, and land use change detection [22]. Sentinel-1 operates at a nominal frequency range C-band (central frequency of 5.404 GHz), the frequency range in which the electromagnetic waves used in radar technology fall is narrowed down from 8 GHz to 4 GHz, corresponding to a wavelength of 3.75 to 7.5 cm.

2.2. Earthquakes dataset

Earthquake datasets contain information about the earthquake's location, depth, magnitude, and source. These datasets can be used for various purposes, such as predicting future earthquakes, assessing their damage potential, and understanding the physics of the process. Multiple sources are available for earthquake datasets, including government agencies, research institutes, and universities. The USGS Earthquake Hazards Program comprehensively collects data from various locations globally. The dataset formats GeoJSON, QuakeML, CSV, and KMLmaking are readily attainable.

3. Theoretical framework:

InSAR is a significant strategy for noticing ground developments brought about by tremors. This method includes looking for sets of radar pictures taken at different times, surveying their stage distinctions, and registering the varieties on the earth's surface and the distance between the satellite. The data collected can create deformation maps that display horizontal and vertical displacement and strain [23]. The basic equation used to measure deformation with InSAR is:

$$\Delta\Phi = (4\pi/\lambda) * \Delta h \quad (1)$$

where ΔΦ is the interferometric phase difference of the radar wavelength, and Δh is the ground deformation in the line-of-sight direction (LOS). The difference in phase between two SAR images, the radar wavelength, and the distance variation between the ground and satellite is represented by Δφ. Merging interferograms can be produced a sequence of deformation maps to estimate the deformation preceding and succeeding an earthquake [24]. These calculations offer insights into fault geometry, displacement amount and direction, and deformation range. Furthermore, InSAR can be employed to explore post-seismic deformation and simulate it through rheological models to evaluate the mechanical characteristics of the earth's crust [17] and [25].

4. Methodology

In InSAR, using deformation methodology with Sentinel-1 data regarding earthquakes involves three primary steps that can be easily understood.

1. To acquire Sentinel-1 SAR data, users must access the Copernicus Open Access Hub. This platform allows users to select their preferred location, date range, and product-level to obtain the desired data.
2. The second step of the process involves preparing the gathered data by making corrections for any atmospheric delays, terrain distortions, and orbital errors. This is achieved by implementing a range of corrections, including calibration, multi-looking, filtering, and phase unwrapping.
3. Interferometric processing is a method that employs pre-processed data to develop interferograms. The interferograms are maps displaying the differential phase between two SAR images, indicating any deformation that might have taken place between the two

acquisition periods. Two SAR images were chosen and lined up to produce an interferogram, and their phase difference was determined.
4. Phase-to-Displacement Conversion: The interferometric phase values were converted to displacement values using the interferometric equation, which relates the phase difference to the line-of-sight displacement:

$$\Delta h = \lambda/(4\pi) * \Delta\Phi \quad (2)$$

where Δh is the line-of-sight displacement (LOS), λ is the radar wavelength, and ΔΦ is the phase difference.
5. To create time series information on the earthquake's progress, displacement maps were produced utilizing sundry interferograms gathered over time.
Deformation analysis examines the distortion changes through time to distinguish patterns such as the size, location, and progress of these changes.

The assessment was highly informative in understanding the workings and traits of earthquakes, such as fault structure, movement distribution, and other significant details. Utilizing InSAR deformation through Sentinel-1 data is an effective technique for observing and examining the spatial and time-based alterations linked with earthquakes; it is beneficial for evaluating potential risks and minimizing dangers.

5. Results

5.1. Focal Mechanism

The direction of the rocks' movement can be analyzed to identify the type of fault. There are three main types of faults: normal, reverse, and strike-slip. In a normal fault, the fault moves downward, proportional to the rocks on the other side and the rocks on one side. In a reverse fault, the fault moves upward, proportional to the rocks on the other side and the rocks on one side. In a strike-slip fault, the rocks move horizontally past each other. Table (1) shows the 7.3, 6, and 6.3 Mw earthquake event information. The data is presented in a tabular format with the following parameters:

Table 1: Earthquake focal mechanisms for (7.3, 6, 6.3) Mw events

Date	Time	Latitude	Longitude	Depth	Mw	Strike	Dip	Rake	Strike	Dip	Rake
12-11-2017	18:18	34.911	45.959	19	7.3	32.82	18.69	177.8	124.9	89.3	71.32
25-08-2018	22:13	34.611	46.242	14	6	88.51	89.13	3.68	358.45	86.32	179.13
25-11-2018	16:37	34.360	45.7443	16	6.3	27.06	81.15	172.35	118.24	82.44	8.93

Based on the information, the earthquake occurred on November 25th, 2018, at 16:37:32.830 UTC. The epicenter was located at latitude 34.3609 degrees and longitude 45.7443 degrees, with a depth of 16 km. The seismic event had a moment magnitude of 6.3, and its focal mechanism was characterized by a strike angle of 27.06 degrees, a dip angle of 81.15 degrees, and a rake angle of 172.35 degrees. Additionally, the auxiliary plane exhibited a strike angle of 118.24 degrees, a dip angle of 82.44 degrees, and a rake angle of 8.93 degrees. The fault type of earthquake was associated with a strike-slip fault, Figure (2). The table above details two seismic events on different dates, times, and locations. The first event occurred on November 12th, 2017, at 18:18, with a magnitude of 7.3 and an epicenter located at latitude 34.911 degrees toward north and longitude 45.959 degrees toward east. The earthquake had a depth of 19 km, and the focal mechanism parameters indicate a strike of

32.82 degrees, a dip of 18.69 degrees, a rake of 177.8 degrees for the nodal plane 1, and a strike of 124.9 degrees, a dip of 89.3 degrees, and a rake of 71.32 degrees for the nodal plane 2. The fault type of earthquake was associated with a reverse or thrust fault, Figure (2). The second event occurred on August 25th, 2018, at 22:13, with a magnitude of 6.0, an epicenter at 34.611 degrees, and a longitude of 46.242 degrees. The earthquake had a depth of 14 km, and the focal mechanism parameters indicate a strike of 88.51 degrees, a dip of 89.13 degrees, a rake of 3.68 degrees for the nodal plane 1, and a strike of 358.45 degrees, a dip of 86.32 degrees, and a rake of 179.13 degrees for the nodal plane 2. The fault type of earthquake was associated with a strike-slip fault, Figure (2).

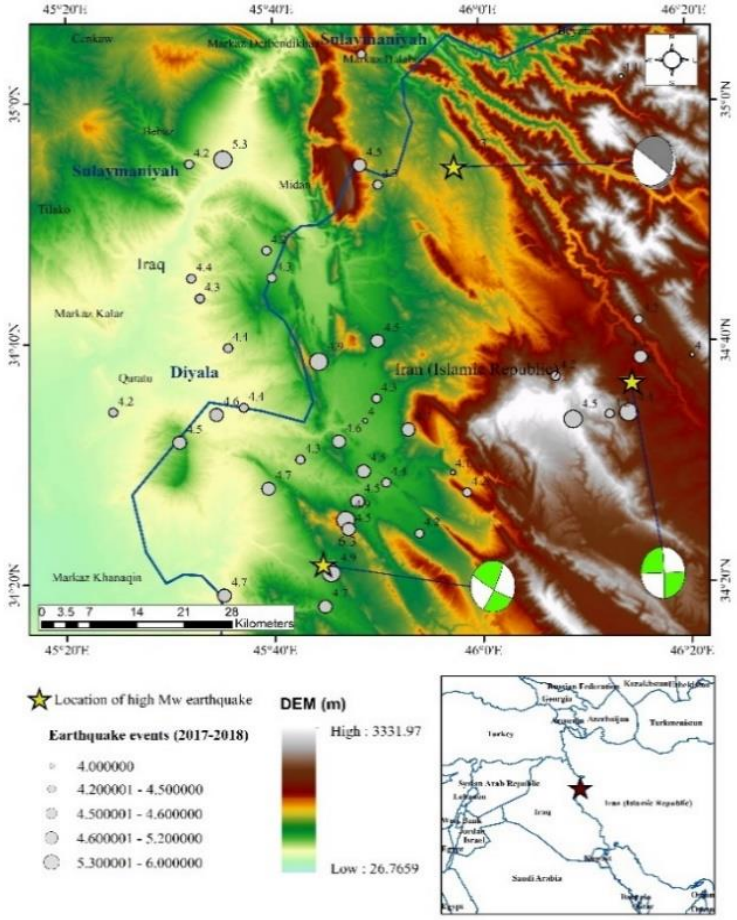

Figure 2: Focal mechanisms solutions (fault type) and digital elevation model (DEM)

5.2. Displacement map

The LOS displacement map for a pair of Sentinel-1 SLC granules was processed using snap software. The pixel values indicate surface movement in meters along the sight line of the sensor. Positive values indicate movement toward the sensor, and negative values indicate movement away from the sensor. The data is in a GeoTIFF file, 32-bit float format, with a projection to WGS 84 / UTM zone 38N and a pixel spacing of 12.5 m. It was generated by applying pre- and post-event processing to a pair of SAR images.

1. S1A_IW_SLC__1SDV_20171111T150004_20171111T150032_019219_0208AF_EE89
2. S1A_IW_SLC__1SDV_20181130T150011_20181130T150038_024819_02BB6F_DFAB

The unwrapped differential phase was converted into measurements of ground movement in meters along the look vector to generate the LOS displacement map. The direction of movement towards the sensor, such as uplift or lateral motion, was indicated by positive

values, whereas movement away from the sensor, such as subsidence or lateral motion, was indicated by negative values. The displacement value of this earthquake was approximately -16 to 90 cm, Figure (3).

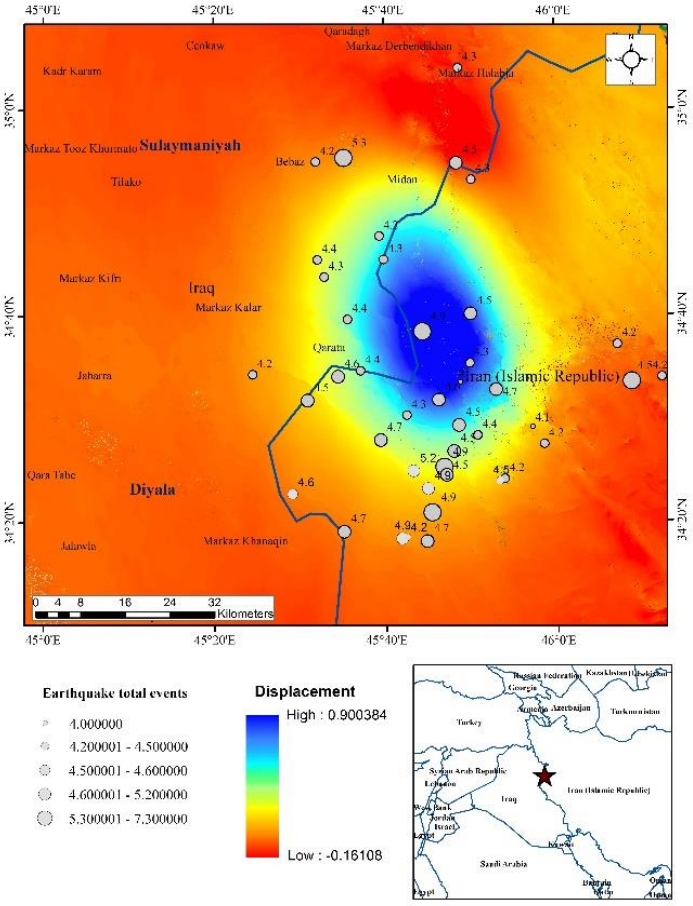

Figure 1: Map of total displacement

5.3. Interferogram analysis

The generated image was based on the phase difference values of the interferogram, which are still wrapped, meaning that they are limited to a range of 2π and; represented by a complete cycle through the color ramp or one "fringe." The fringes were displayed on a background of the backscatter intensity values to give topographic context to the deformation. Since the wrapped interferogram values are on a wrapped 2-pi scale, they were best visualized using a color ramp. Each fringe corresponds to a line-of-sight displacement equal to half of the sensor wavelength. The Sentinel-1 SAR sensor has a wavelength of 5.6 cm; each fringe would represent a line-of-sight displacement of 2.8 cm. Fringes with narrow spacing denote higher deformation levels than those with wider spacing. The Interferogram deformation value of the earthquake events is high, Figure (4).

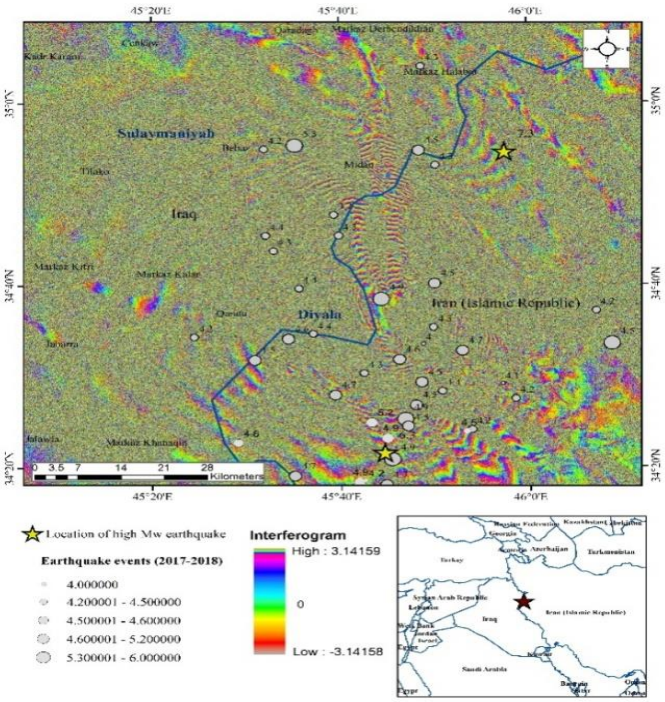

Figure 4: Interferogram for total deformation

6. Discussions

The research paper explains that analyzing different aspects of an earthquake, such as focal mechanism, displacement map, and interferogram analysis, can provide crucial information about the earthquake's characteristics. Focal mechanism analysis determines the type of fault that caused the earthquake, with the November 25th, 2018, earthquake having a strike-slip fault, while the November 12th, 2017, earthquake had a reverse or thrust fault. Displacement map analysis uses Sentinel-1 SLC granules processed using snap software to show surface movement in meters along the sensor's sight line. The November 25th, 2018, earthquake caused a displacement value of approximately -17 to 87 cm, which can help identify areas that experienced significant ground movement. Interferogram analysis uses the interferogram phase difference values to generate an image that provides information about the extent and magnitude of ground deformation caused by the earthquake. Fringes with smaller spacing indicate higher levels of deformation than fringes with wider spacing. Analyzing different aspects can help assess an earthquake's impact and develop effective measures to mitigate its effects.

7. Conclusions

The provided information emphasizes the significance of comprehensive earthquake analysis to gain insights into their attributes, ultimately aiding in mitigating their adverse impacts. The earthquake-occurrence way offers crucial insights into the underlying fault responsible for it. Such information plays a pivotal role in predicting future earthquakes in the same region. The displacement map can identify locations that experienced significant ground movements, such as uplift or subsidence, which can impact infrastructure and buildings. Interferogram analysis is a valuable technique that provides comprehensive information on ground deformation. It can prove to be an immense help in rescue and relief operations during natural calamities. Moreover, the analysis can assist in devising effective strategies to minimize the damage caused by earthquakes to human lives and infrastructure in the future. In summary, an in-depth analysis of earthquakes is essential for building a resilient society and minimizing the damage caused by natural disasters.

Acknowledgments

The authors express gratitude to various institutions for their research contributions. The Lab. of Seismology and Spatial Data Analysis at the University of Baghdad and the Seismic Monitoring Laboratory at the University of Basrah provided expertise and collaboration on seismic activity. The research relied significantly on data, expertise, and analytical tools provided by the United States Geological Survey, the ESA, and the ASF. The authors are thankful for the support and assistance of these institutions and anticipate continued collaborations with them in the future.

References:

[1] B. Zhang, G. Xu, Z. Lu, Y. He, M. Peng, and X. Feng, "Coseismic deformation mechanisms of the 2021 ms 6.4 yangbi earthquake, Yunnan province, using InSAR observations," *Remote Sens.*, vol. 13, no. 19, pp. 1–14, 2021, doi: 10.3390/rs13193961.

[2] J. Yang, C. Xu, Y. Wen, and G. Xu, "Complex Coseismic and Postseismic Faulting During the 2021 Northern Thessaly (Greece) Earthquake Sequence Illuminated by InSAR Observations," *Geophys. Res. Lett.*, vol. 49, no. 8, pp. 1–10, 2022, doi: 10.1029/2022GL098545.

[3] Y. Chen, Y. Hu, L. Qian, and G. Meng, "Early Postseismic Deformation of the 2010 Mw 6.9 Yushu Earthquake and Its Implication for Lithospheric Rheological Properties," *Geophys. Res. Lett.*, vol. 49, no. 15, 2022, doi: 10.1029/2022GL098942.

[4] M. Matsuoka and N. Nojima, "Building damage estimation by integration of seismic intensity information and satellite L-band SAR imagery," *Remote Sens.*, vol. 2, no. 9, pp. 2111–2126, 2010, doi: 10.3390/rs2092111.

[5] H. M. Al-Samarrai and M. H. Al-Jiboori, "Prediction of Daily Maximum Air Temperature for Transitional Seasons by Statistical Methods in Baghdad," *Iraqi J. Sci.*, pp. 2085–2094, Apr. 2023, doi: 10.24996/ijs.2023.64.4.42.

[6] X. Tong, X. Xu, and S. Chen, "Coseismic Slip Model of the 2021 Maduo Earthquake, China from Sentinel-1 InSAR Observation," *Remote Sens.*, vol. 14, no. 3, pp. 1–10, 2022, doi: 10.3390/rs14030436.

[7] L. El hani and A. Bouberria, "The Use of Remote Sensing and GIS in Studying the Dynamics of Irrigated Space in Guercif Plain (Morocco)," *Iraqi J. Sci.*, pp. 2060–2069, Apr. 2023, doi: 10.24996/ijs.2023.64.4.40.

[8] M. Motagh, J. Beavan, E. J. Fielding, and M. Haghshenas, "Postseismic Ground Deformation Following the September 2010 Darfield, New Zealand, Earthquake From TerraSAR-X, COSMO-SkyMed, and ALOS InSAR," *IEEE Geosci. Remote Sens. Lett.*, vol. 11, no. 1, pp. 186–190, Jan. 2014, doi: 10.1109/LGRS.2013.2251858.

[9] G. Feng, E. A. Hetland, X. Ding, Z. Li, and L. Zhang, "Coseismic fault slip of the 2008 Mw 7.9 Wenchuan earthquake estimated from InSAR and GPS measurements," *Geophys. Res. Lett.*, vol. 37, no. 1, pp. 1–5, 2010, doi: 10.1029/2009GL041213.

[10] R. Jolivet and M. Simons, "A Multipixel Time Series Analysis Method Accounting for Ground Motion, Atmospheric Noise, and Orbital Errors," *Geophys. Res. Lett.*, vol. 45, no. 4, pp. 1814–1824, 2018, doi: 10.1002/2017GL076533.

[11] Z. Jin and Y. Fialko, "Coseismic and Early Postseismic Deformation Due to the 2021 M7.4 Maduo (China) Earthquake," *Geophys. Res. Lett.*, vol. 48, no. 21, pp. 1–10, 2021, doi: 10.1029/2021GL095213.

[12] M. Zhu, F. Chen, W. Zhou, H. Lin, I. Parcharidis, and J. Luo, "Two-Dimensional InSAR Monitoring of the Co- and Post-Seismic Ground Deformation of the 2021 Mw 5.9 Arkalochori (Greece) Earthquake and Its Impact on the Deformations of the Heraklion City Wall Relic," *Remote Sens.*, vol. 14, no. 20, 2022, doi: 10.3390/rs14205212.

[13] H. A. Rasheed and A. H. Shaban, "Evaluate the pollution of underground water by multi sub-kriging interpolation methods," 2022, p. 020072. doi: 10.1063/5.0092310.

[14] H. K. Hassun, B. H. Hussein, E. M. T. Salman, and A. H. Shaban, "Photoelectric properties of SnO2: Ag/P–Si heterojunction photodetector," *Energy Reports*, vol. 6, pp. 46–54, Feb. 2020, doi: 10.1016/j.egyr.2019.10.017.

[15] A. H. Shaban, A. K. Resen, and N. Bassil, "Weibull parameters evaluation by different methods for windmills farms," *Energy Reports*, vol. 6, pp. 188–199, Feb. 2020, doi: 10.1016/j.egyr.2019.10.037.

[16] H. A. Rasheed and A. H. Shaban, "The best interpolation methods for evaluate water table pollution," 2022, p. 020074. doi: 10.1063/5.0094195.

[17] H. H. M. Wathiq Abdulnaby, Maher Mahdi, Rafed Al-Mohmed, "Seismotectonics of Badra-Amarah Fault, Iraq-Iran Border," *IOSR J. Appl. Geol. Geophys.*, vol. 4, no. 3, pp. 27–33, 2016, doi: 10.9790/0990-0403022733.

[18] M. S. Shimal and A. H. Shaban, "Evaluation of the Pollution Elements at Samara Water Table â€" Iraq," *Iraqi J. Sci.*, pp. 898–907, Apr. 2020, doi: 10.24996/ijs.2020.61.4.23.

[19] H. A. Rasheed and A. H. Shaban, "Evaluate the Distribution of Heavy Elements that Dissolved in Ground Water Using IDW in AL-Wafa City, Al-Ramadi, Iraq," *Iraqi J. Phys.*, vol. 19, no. 51, pp. 7–14, Dec. 2021, doi: 10.30723/ijp.v19i51.690.

[20] R. A. Abtan, A. H. Al-Saleh, H. J. Mohamed, H. K. Abbas, and A. Alzuky, "Texture Features of Grey Level Size Zone Matrix for Breast Cancer Detection," *Iraqi J. Sci.*, pp. 492–502, Jan. 2023, doi: 10.24996/ijs.2023.64.1.43.

[21] F. K. Mashee, "Estimation the blast wave pressure effecters by apply Remote Sensing (RS) and Geographic Information System (GIS) techniques," *Iraqi J. Phys.*, vol. 15, no. 34, pp. 87–98, 2019, doi: 10.30723/ijp.v15i34.124.

[22] Z. K. I. A. B. Fouad K. Mashee Al Ramahi, "Estimation of Suaeda aegyptiaca Plant distribution regions at Iraq using RS & GIS Applications," *Iraqi J. Sci.*, vol. 58, no. 2A, pp. 767–777, 2017.

[23] A. Mehrabi *et al.*, "Incorporating persistent scatterer interferometry and radon anomaly to understand the anar fault mechanism and observing new evidence of intensified activity," *Remote Sens.*, vol. 13, no. 11, pp. 1–22, 2021, doi: 10.3390/rs13112072.

[24] A. Tronin, "Satellite Remote Sensing in Seismology. A Review," *Remote Sens.*, vol. 2, no. 1, pp. 124–150, Dec. 2009, doi: 10.3390/rs2010124.

[25] Z. Jin and Y. Fialko, "Coseismic and Early Postseismic Deformation Due to the 2021 M7.4 Maduo (China) Earthquake," *Geophys. Res. Lett.*, vol. 48, no. 21, Nov. 2021, doi: 10.1029/2021GL095213.